Icarus **141**, 156–171 (1999)
Article ID icar.1999.6141, available online at http://www.idealibrary.com on IDEAL®

Radar Scattering from a Self-Affine Fractal Surface: Near-Nadir Regime

Michael K. Shepard

Department of Geography and Earth Science, 400 E. Second Street, Bloomsburg University, Bloomsburg, Pennsylvania 17815
E-mail: mshepard@bloomu.edu

and

Bruce A. Campbell

Center for Earth and Planetary Studies, National Air and Space Museum, MRC 315, Smithsonian Institution, Washington, DC 20005

Received June 29, 1998; revised April 8, 1999

Planetary surfaces are better described by nonstationary fractal statistics than those more commonly assumed in current radar scattering models. Therefore, we have developed a radar scattering model applicable to self-affine fractal surfaces when observed near-nadir. The model predicts a family of angular scattering functions that smoothly transition between forms similar to the commonly utilized Hagfors, Gaussian, and exponential surface models. The model predicts that the near-nadir scattering behavior is determined by the wavelength-scaled roughness, i.e., the roughness that would be measured by a field worker using a ruler one wavelength in size, and the surface scaling behavior described by the fractal dimension or Hurst exponent. Additionally, this model predicts that the scattering behavior should scale with wavelength in a self-affine manner, i.e., the scattering behavior at long wavelengths should look "smoother" than that at short wavelengths. The scattering behavior predicted by the model is consistent with that observed for Venus by the Magellan altimeter experiment.

Key Words: **radar; surfaces/planets; venus/surface.**

I. INTRODUCTION

The topography of natural surfaces at scales of a few meters or less is often referred to as roughness and is of fundamental importance to the interpretation of geologic emplacement mechanisms and modification processes. Because there are few instances of *in situ* measurements on the terrestrial planets, the planetary community relies extensively upon remote observations to determine surface roughness and to infer geologic structure, processes, and history. While surface roughness is important at all wavelengths, its effect on scattering behavior in the microwave (radar) spectrum is of particular interest. The scales of roughness contributing to microwave scattering are in the centimeter to tens of meters range—the same scales at which many important geologic properties are manifest. Furthermore, compositional variations generally (although not always) play only a minor role in surface scattering properties at microwave frequencies.

One of the primary difficulties experienced by those using microwave data is the physical interpretation of roughness parameters extracted from scattering observations. For example, one model used extensively by the planetary community is the Hagfors (1964) model for quasi-specular scattering. Its popularity stems from its ability to consistently fit many near-nadir (backscattering angle, $\theta < \sim 20^\circ$) backscatter observations. The roughness parameter extracted from this model is C, and it is generally agreed (Tyler *et al.* 1992) that $C^{1/2}$ is a measure of the root-mean-square (RMS) surface slope at scales that are large compared with the wavelength. It is not uncommon to see Hagfors parameters of $C = 100$ reported in the literature, corresponding to RMS slopes of about 6°. *Interpreting* this value in a quantitative fashion is the difficulty. What surfaces on the Earth have RMS slopes of 6°? If the profile of a terrestrial analog surface were supplied, how would this value be measured? What does this value imply about the surface geology?

The shape of the angular scattering function and the type of surface statistics inferred from its behavior are also of interest for their geologic implications. For example, studies done by Simpson and Tyler (1982) and Tyler *et al.* (1992) suggest that the meter-scale surface statistics of the Moon and Venus are significantly different. On the Moon, the majority of near-nadir observations are best fit by a Hagfors (1964) model, while on Venus the most common best-fit model has an exponential form. Tyler *et al.* (1992) hypothesize that this reflects differences in the processes of erosion and deposition on the two planets. Beyond this, little is understood about why these scattering differences exist and how they can be exploited to provide new geologic insights. Several workers have noted a wavelength dependence in the RMS slope inferred from near-nadir echoes (Hagfors and Evans 1968, Muhleman 1964, Simpson and Tyler 1982). It has long been recognized that surfaces appear smoother at longer wavelengths than at shorter wavelengths, but there has been little

0019-1035/99 $30.00

progress in quantifying this behavior or interpreting it in terms of surface geology.

In this paper, we derive a radar scattering model which is capable of quantitatively addressing each of the above problems. Our derivation involves two new assumptions that fundamentally differ from previous work. First, we assume that the surface topography is represented by a random, isotropic, self-affine fractal surface. Fractal surfaces are, by definition, nonstationary, and utilize a scale-dependent roughness parameter. Previous models have assumed the surface roughness to be stationary and have lacked any explicit scale-dependent measures. We discuss and justify this assumption below at some length.

Our second major departure from earlier work is the assumption that the surface is rough at all scales. Previous work (Beckmann and Spizzichino 1963, Hagfors 1964, etc.) assumed that the surface is smooth or gently undulating at the scale of the wavelength. This allowed traditional ray or physical optics methods and equations to be utilized, including the well-known Fresnel reflection equations for smooth surfaces. While the assumption of a smooth surface at the wavelength scale is mathematically convenient, it is probably not realistic for most planetary surfaces. In order to make our assumption mathematically tractable, we treat the scattering process as one of diffraction rather than reflection. This is essentially a physical optics approach in which each point of the surface is modeled as an independent source of Huygens spherical wavelets, i.e., isotropic electric-field wavelets. The trade-off is that this methodology, while mathematically convenient, is only an approximation since it does not allow for a rigorous treatment of the electromagnetic field at the boundary. However, it does lead to new insights into the scattering process and explains many of the problems discussed previously.

In the next section we review previous efforts to model radar scattering in the near-nadir regime. Following that, we provide a review of and justification for self-affine topography models. We then derive the scattering model and follow with a discussion of the following topics: the physical meaning of the inferred surface roughness parameter, the variety in angular scattering "shapes," and the wavelength dependence of the near-nadir echo. In the final section of this paper, we illustrate the inverse problem using near-nadir observations of Venus. Throughout, we will illustrate concepts using both synthetic and real topographic profiles.

II. PREVIOUS MODELS

Microwave scattering models developed for near-nadir ($\theta < \sim 20^\circ$) planetary applications have generally taken two different approaches, namely geometric and physical optics (cf. Barrick and Peake 1967, or Tyler *et al.* 1992, for a historical review). All of the models currently in use make a tangent plane assumption, i.e., a smooth surface at the scale of the wavelength, and are collectively referred to as "quasi-specular" models. Unfortunately, this term has become synonymous with scattering in the near-nadir direction, even though it implies a particular kind of scattering mechanism. We do not make the tangent plane assumption in our model and therefore will refer to all scattering models at this geometry as "near-nadir."

The most intuitive of the near-nadir models utilizes a geometric optics approach. The surface is treated as a collection of facets, large with respect to the wavelength and oriented with some statistical distribution, typically of a Gaussian or exponential form (Hagfors and Evans 1968, Simpson and Tyler 1982, Tyler *et al.* 1992). Each facet is assumed to be smooth at the scale of the wavelength and therefore to coherently (i.e., specularly) reflect incident power according to the Fresnel power reflection equations for smooth surfaces. The near-nadir echo is the incoherent sum (sum of powers, not of electromagnetic fields) of reflections from those facets oriented in such a way as to specularly reflect back to the receiver. Interference effects from adjacent facets are assumed to be negligible. In this model, the angular scattering function is proportional to the probability distribution of surface slopes that are large and smooth with respect to the wavelength. Muhlemann (1964) utilized a similar approach, but modeled the facets as the combination of both a random height and a horizontal scattering length variable. His mean surface slope is defined as the ratio of the standard deviations of these two variables. This latter model has been particularly successful in reproducing the scattering behavior for Venus at large scattering angles ($>20^\circ$), although the best-fit parameters are strictly empirical (Tyler *et al.* 1992).

The second approach to modeling near-nadir scattering utilizes principles of physical optics. Here, the near-nadir echo is modeled as the sum of the incident and reflected electromagnetic fields from a gently undulating surface. Again, it is generally assumed that the surface is smooth at the wavelenth scale so the Fresnel equations can be used to model the power reflection coefficient. The surface topography is assumed to have a stationary random distribution of heights about some mean, commonly a Gaussian distribution. In addition, an assumption is made regarding the correlation between adjacent points; common forms for this "autocorrelation" function include the Gaussian and exponential. Hagfors (1964) derived a model of this type, but assumed a linear autocorrelation function near the origin. This latter assumption and subsequent model have been strongly criticized on mathematical and physical grounds (Barrick 1970); however, the Hagfors model is still widely utilized because it appears to accurately fit observed near-nadir scattering behavior (Simpson and Tyler 1982, Tyler *et al.* 1992).

III. SELF-AFFINE TOPOGRAPHY

A. *The Need for a New Surface Roughness Paradigm*

All of the radar scattering models discussed above assume a stationary surface, i.e., a surface with statistical properties that are invariant with respect to scale and position. Stationarity is most commonly invoked by the assumption that the RMS height of a surface is a constant, and throughout the remainder of this

paper we shall use the term "stationary" to refer to this specific assumption.

Recent work by Sayles and Thomas (1978), Mandelbrot (1982), and many others has conclusively demonstrated that, contrary to the above assumptions, natural surfaces are not stationary and are more appropriately described by fractal (power-law) statistics. Figure 1 illustrates how commonly measured quantities such as RMS height, slope, and autocorrelation length vary with scale for a typical young basalt flow measured during the Geologic Remote Sensing Field Experiment (Arvidson *et al.* 1991, Shepard *et al.* 1995). Both the autocorrelation length and the RMS height increase as the profile sample length is increased, while RMS slope decreases with increasing scale or step size (we shall discuss exactly how these curves were generated below). Similar behavior is observed for many other geologic surfaces.

If we desire to extract meaningful geological information from microwave observations, we must incorporate a more realistic model for surface roughness/topography in our scattering models. We suggest that many of the difficulties experienced in quantitatively interpreting near-nadir observations are due to unrealistic surface models–models that neither explicitly account for the scale-dependent roughness of the surface nor recognize its intrinsic power-law (fractal) behavior. We therefore adopt a self-affine surface roughness model in this work and derive a near-nadir scattering model based on that premise. Below, we briefly outline the mathematical properties of self-affine surfaces and further justify our adoption of this model.

B. Description of Self-Affine Fractal Topography

In fractal statistics, there are defined two basic types of scaling behavior—self-similar and self-affine. Self-similar fractals were introduced by Mandelbrot (1967) in his classic study of the length of the British coastline. One of the major points of that study was that the coastline was statistically indistinguishable at any scale, i.e., without a labeled scale in the image, one could not tell whether one was looking at kilometer- or centimeter-scale versions of the coast. A self-affine fractal is one which scales differently in orthogonal dimensions and therefore has an intrinsic scale dependence. In general, a self-affine surface (or profile of that surface) does not roughen in the vertical direction as quickly as the horizontal scale increases, and therein lies the major difference between self-similarity and self-affinity.

As an example, consider an island uniformly covered by a grass lawn. From a few hundred meters altitude, the surface appears extremely smooth and the island perimeter, or coastline, appears ragged. If we take the perspective of an ant on the coastline, however, the grass surface now appears incredibly rough vertically, but the (horizontal) perimeter has the same ragged appearance. In other words, zooming in does not change the appearance of the island perimeter (self-similarity), but has a substantial effect on the surface topography or roughness (self-affinity). Surface topography falls exclusively within the realm of random self-affine fractals, and it is this type of fractal measure that we shall utilize throughout this paper.

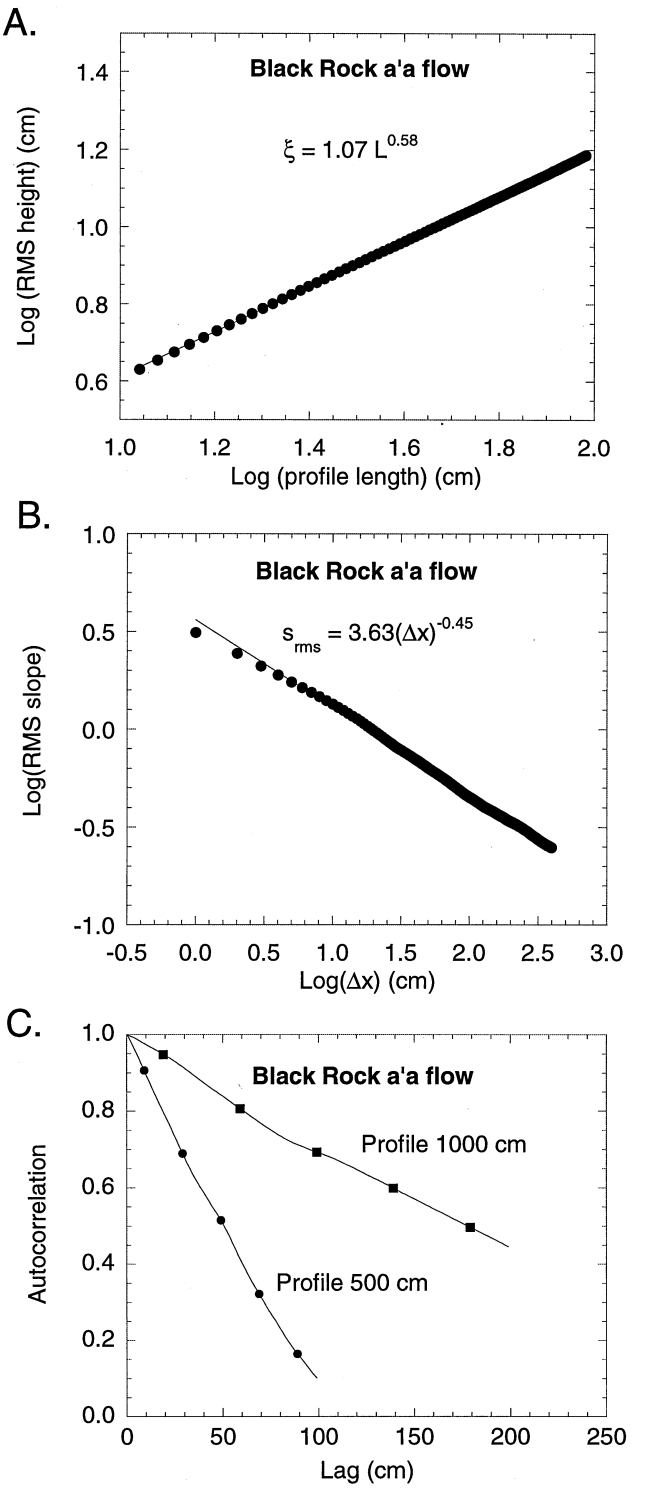

FIG. 1. (A) Log–log plot of relationship between RMS height and profile length for the Black Rock lava flow, Lunar Crater Volcanic Field, Nevada. Each point is the average RMS height for all possible profile samples of length, L. (B) Log–log plot of relationship between RMS slope and step length for the Black Rock lava flow, Lunar Crater Volcanic Field, Nevada. As in (A), each point is the average RMS slope for all possible slopes measured at length Δx. (C) Autocorrelation function for two different profile lengths, Black Rock lava flow, Lunar Crater Volcanic Field, Nevada.

For a surface, we define x and y to be the (orthogonal) horizontal coordinates of a point, and z to be the vertical coordinate, or height, at that point. For a profile sample of length, L, we use x as the horizontal coordinate, and again, z as the vertical coordinate. There are several surface parameters commonly measured by field workers (typically along profiles or transects), and we now examine each of these and their behavior on a self-affine surface. For each surface, we assume the mean height to be constant, and for convenience will often assume it to be zero. Throughout this discussion, we will frequently refer to a surface or a profile of that surface interchangeably; the concepts are the same for each, but profiles are more commonly measured.

The most commonly measured surface parameter (other than the mean) is the RMS height, or standard deviation, ξ,

$$\xi(L) = [\langle (z - \bar{z})^2 \rangle]^{1/2}. \tag{1a}$$

Here, the angle brackets indicate the expectation value, or weighted average, over all possible values of z within a sample profile of length, L. (*Note*: We use the symbol ξ instead of the more familiar σ and reserve σ for radar backscatter cross-section.) For a stationary surface, such as white noise, ξ is independent of the length of the profile over which it is measured. For a self-affine profile or surface, ξ is a function of the sample length over which it is measured (Hastings and Sugihara 1993, Shepard *et al.* 1995, Campbell and Shepard 1996):

$$\xi(L) = \xi(L_0)\left(\frac{L}{L_0}\right)^H = \xi_0\left(\frac{L}{L_0}\right)^H. \tag{2a}$$

L_0 is a standardized reference length and H is a constant, the Hurst exponent, and is discussed at length below. As illustrated in Fig. 1, RMS height increases with increasing sample length on a fractal profile. For clarity, each point in that figure is the average of the RMS heights measured over all possible profiles of length, L. For each possible profile, the mean height, $\bar{z}$, which is used to compute the RMS height [Eq. (1a)], is a local mean, i.e., the mean of each individual profile.

A second parameter, less commonly measured, is the RMS deviation (also referred to as structure function, variogram, Allan deviation), ν,

$$\nu(\Delta x) = [\langle (z(x) - z(x + \Delta x))^2 \rangle]^{1/2}. \tag{1b}$$

In essence, this parameter is a measure of the difference in height between points separated by a distance, Δx. For a stationary surface, ν is, again, a constant. For a self-affine surface

$$\nu(\Delta x) = \nu(\Delta x_0)\left(\frac{\Delta x}{\Delta x_0}\right)^H = \nu_0\left(\frac{\Delta x}{\Delta x_0}\right)^H, \tag{2b}$$

analogous to the RMS height. The term Δx_0 is a reference step size. Unlike the RMS height, the RMS deviation is independent of the length of the profile over which it is measured—it is only a function of the step interval between two points on any given profile.

The RMS deviation is frequently measured as an intermediate to the RMS slope, s,

$$s(\Delta x) = \frac{\nu(\Delta x)}{\Delta x}. \tag{1c}$$

Although ν is a constant on a stationary surface, s is not and falls off as $1/\Delta x$. For a self-affine surface, RMS slope also falls off with increasing step size, but at a rate dependent upon H,

$$s(\Delta x) = s(\Delta x_0)\left(\frac{\Delta x}{\Delta x_0}\right)^{H-1} = s_0\left(\frac{\Delta x}{\Delta x_0}\right)^{H-1}. \tag{2c}$$

In Eqs. (2), $\xi(L_0) = \xi_0$, $\nu(\Delta x_0) = \nu_0$, and $s(\Delta x_0) = s_0$ are common roughness parameters anchored at a specific reference scale, and H is a parameter that describes how these values change with scale, $0 \le H \le 1$. There are several H parameters in the literature which have similar or analogous meanings and are often confused with one another, among them the Hurst exponent, Hausdorff measure, and Holden exponent (Falconer 1990, Hastings and Sugihara 1993, Shepard *et al.* 1995, Mandelbrot and Wallis 1995, Turcotte 1997). In order to maintain consistency with previous work (Hastings and Sugihara 1993, Shepard *et al.* 1995, Campbell and Shepard 1996), we will refer to H as the Hurst exponent.

To illustrate the role of the Hurst exponent, Fig. 2 shows three synthetic self-affine profiles, each of which have the same value of s_0 (in this case the RMS slope at the smallest facet scale) but differ in their Hurst exponents. If one were to zoom in to each of these profiles, they would be difficult to tell apart because the roughness at small scales is the same for each profile. However,

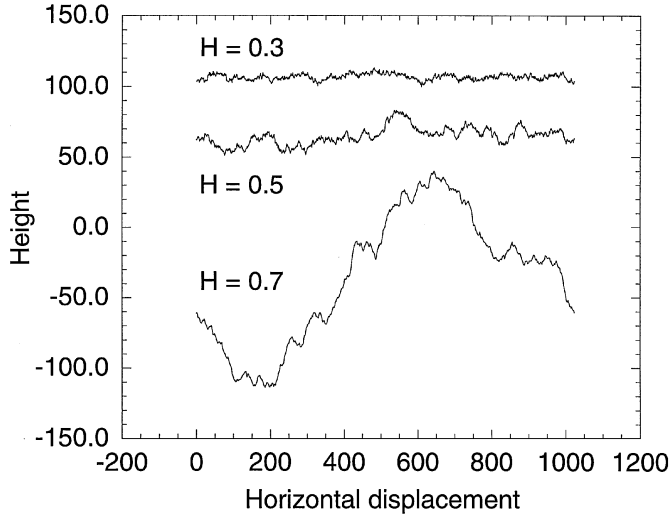

FIG. 2. Three self-affine profiles, each with the same RMS slope at the smallest scale (1 unit on x axis), but differing in their Hurst exponents. Although each profile has the same small scale roughness, the large scale roughness increases with increasing H.

at larger scales, the profiles change dramatically. Note that the profile with the smallest value of H is relatively smooth at large scales; i.e., the RMS height does not increase rapidly with scale. Conversely, the profile with the largest value of H is relatively rough at all scales because its RMS height *does* rapidly increase with increasing horizontal scale.

There are three "endmember" self-affine behaviors worth noting: $H = 0.0$, 0.5, and 1.0. In the case of $H = 0.0$, Eqs. (2) show that the RMS height and deviation are independent of the length of the profile from which they are measured, while the RMS slope decreases hyperbolically ($1/x$) with scale. This case, then, illustrates a form of stationary behavior, somewhat analogous to white noise [it is actually referred to as pink or $1/f$ noise in the engineering community (Schroeder 1991)]. The case of $H = 0.5$ is very commonly observed in nature and is often referred to as Brownian noise (Schroeder 1991, Turcotte 1997). On a Brownian profile, the RMS height and deviation scale as the square root of the horizontal scale. The case of $H = 1.0$ is a form of self-similar behavior. Examination of Eq. (2c) shows that the RMS slope is constant at all scales (thus the term "self-similar") while the RMS height and deviation increase at the same rate as the horizontal axes.

Another interesting characteristic of these endmember cases relates to their "persistence" (Malamud and Turcotte 1998, Turcotte 1997). Surfaces or profiles with $H < 0.5$ are said to be anti-persistent; i.e., if the general trend of the profile in the past has been in one direction, there is a greater than average chance that the profile will change direction in the immediate future. This gives rise to a very jagged appearance to these surfaces at small scales; however, over the long term these trends tend to cancel and so the entire surface never deviates far from the mean (Fig. 2). Surfaces with $H > 0.5$ are said to be persistent; i.e., future trends will tend to be the same as past trends. At the small scale, these surfaces appear to be fairly smooth, but over the long term become quite rough and rolling in appearance (Fig. 2). Brownian surfaces ($H = 0.5$) have no persistence—future behavior is independent of past behavior (Fig. 2).

The Hurst exponent, H, is related to the commonly reported fractal dimension, D, by

$$\begin{aligned} D &= 2 - H \\ D &= 3 - H. \end{aligned} \tag{3}$$

The first expression in Eq. (3) is applicable to a profile, and the second is applicable to a surface (Hastings and Sugihara 1993, Shepard *et al.* 1995, Turcotte 1997). In this paper, we will primarily utilize the Hurst exponent instead of the fractal dimension; it minimizes the size of the derived equations and avoids the confusion that sometimes arises when alternately discussing the roughness of profiles and surfaces in terms of fractal dimension.

C. Justification for Assumption of Self-Affine Behavior

It is not well understood why natural surfaces obey the relationships (or derivatives of them) expressed by Eqs. (2); the empirical evidence that that they do, however, is overwhelming. Figure 1 illustrates this behavior for a basalt flow; both the RMS height and the RMS slope obey the scaling relationships of Eqs. (2) with $H \sim 0.6$. Mark and Aronson (1984) report values of H ranging from 0.1 to 0.96 for a variety of geologic provinces at scales ranging from tens of meters to tens of kilometers. Brown and Scholz (1985) report H values ranging from $\sim$0.4 to 1.0 for rock surfaces measured at scales of micrometers to centimeters. Our own work with numerous lava flows yielded H values from 0.25 to 0.75 at scales of centimeters to tens of meters (Campbell and Shepard 1996). Farr (1992) found $H \sim 0.5$ on a wide range of geologic surfaces, also at scales of centimeters to tens of meters. Recent work on the terrestrial planets has shown similar behavior. Haldemann *et al.* (1997, personal communication) found $H \sim 0.5$ for the terrain around the Mars Pathfinder landing site at scales of centimeters to tens of meters, while Helfenstein and Shepard (1999) report H values of 0.5–0.7 for undisturbed lunar regolith at scales of submillimeters to centimeters.

While the Hurst exponents of natural terrain tend to cluster about $H = 0.5$ (Brownian noise), the roughness of surfaces at any standardized length scale spans an enormous range of values. Basaltic lava flows measured in Hawaii display a range of RMS heights on 1-m profiles, from $\sim$8 cm for rough a'a flows to $<$1 cm for very smooth pahoehoe flows. RMS slopes at 1 m scale for these same flows ranged from 0.23 ($\sim 13^\circ$) to 0.04 ($\sim 2^\circ$). The smoothest site for which we have topographic data is the Lunar Lake playa, Nevada, with an RMS slope of $\sim 1^\circ$ or less at the 1-m scale, while one of the roughest sites we have investigated is the a'a flow in Fig. 1, also in the Lunar Crater Volcanic Field, which has an RMS slope of $\sim 25^\circ$ at the 1-m scale (Arvidson *et al.* 1991, Shepard *et al.* 1995). J. Plaut (1998, personal communication) has measured RMS slopes as high as 40° at the 1-m scale on rhyolitic flows at Inyo Domes, California. While this list of examples is far from exhaustive, it does give a sense for the range of surface roughness values that may reasonably be encountered.

In several instances, we have noted that a single Hurst exponent is insufficient to describe the scaling behavior of a surface (Campbell and Shepard 1996). In these cases, we find that different Hurst exponents are valid at different ranges of scale, or more generally, that H has a piecewise functional dependence on scale. This behavior is thought to be caused by different physical processes operating at different scales; e.g., for lava flows, meter scale properties are controlled by magma characteristics and emplacement rates while centimeter scale properties are dominated by weathering rates and styles (cf. Campbell and Shepard 1996). The most realistic treatment of natural surfaces should include this behavior. While this is readily implemented in the model derived below, we limit our discussion to cases in which H can be assumed constant over the range of scales which dominate the radar scattering process.

Finally, we note that a purely self-affine surface cannot exist in nature. A quick examination of Eqs. (2) shows that the RMS slope approaches infinity as the scale decreases to zero and the

RMS height and deviation approach infinity as the length scale increases without bound. There obviously must be maximum and minimum scales beyond which a fractal model (with a single Hurst exponent) breaks down. However, over the range of scales we are interested in, from one or more orders of magnitude smaller than a typical radar wavelength to an order of or more magnitudes larger than a wavelength, most surfaces can be realistically treated as self-affine and modeled with a constant Hurst exponent.

IV. MODEL DERIVATION

A. Assumptions and Terminology

The following assumptions are utilized in our model derivation.

(1) The surface can be described as an azimuthally isotropic self-affine surface described by a single Hurst exponent, H, and vertical roughness parameter (RMS height, deviation, or slope) at a known horizontal scale. The height distribution at all scales is Gaussian.

(2) The surface is rough at horizontal scales ranging from several orders of magnitude smaller to several orders of magnitude larger than the wavelength, i.e., not necessarily gently undulating. (Note that this implies that the surface area dimensions are much larger than the incident wavelength.)

(3) The incident wave is of wavelength λ and is planar, implying a distant radar source.

(4) The receiver is in the far-field or Fraunhofer zone.

(5) Each point of the surface independently reradiates, or singly scatters, the incident energy as a spherical wave, or Huygens wavelet, with magnitude proportional to the bulk properties (i.e., dielectric constant) of the surface. All points are further assumed to have identical electric-field amplitudes in the chosen polarization state and a phase determined only by the relative height of the surface. This representation will not lead to a rigorously correct analysis of the scattered electric field above the surface, as it ignores point-to-point coupling and preferential polarization of the reflected wave due to local surface tilt or discrete structures (cracks, edges, vesicles, etc.). In previous physical optics models, this assumption was validated by stipulating the surface to be gently undulating or well behaved in the vicinity of the scattering point. Here, we make no such stipulation—real surfaces do not behave in this fashion. Instead, we will argue below that the use of a scale-dependent roughness parameter allows us to plausibly invoke a smoothing behavior in the reradiated field at smaller horizontal (and vertical) scales, similar to that first propounded by Hagfors (1964). It is also a necessary approximation to make the solution mathematically tractable.

(6) Because our derivation utilizes Huygens wavelets, we implicitly assume the electromagnetic field to be scalar and ignore depolarization effects; i.e., if the incident field is horizontally polarized, we assume the reradiated field is also horizontally polarized. Again, this is a convenient approximation. In reality, each point will have a scattered field which is partially depolarized by surface roughness and by internal scattering within the target material. The observed like-polarized (HH, VV, LR, or RL) echo will thus be less than that predicted by the simple Huygens radiator case by some unknown amount. However, as long as the polarization state of each point is a random function of the surface height (e.g., discrete linear elements do not occur solely at the tops of hills), then we may take the net effect of depolarization into the "effective reflectivity" of the surface.

(7) Multiple scattering between adjacent points is ignored. This will be a reasonable assumption for most rocky surfaces, where approximately 5–20% of the incident power is singly scattered. However, it will become an increasingly poor assumption for radar bright regions, such as the venusian highlands.

Throughout the following discussion, we will treat the process of scattering from a surface of arbitrary shape to be equivalent to the process of diffraction through an aperture or radiation from an antenna of the same shape. The mathematics of these processes are virtually identical. The surface area under consideration is assumed to be azimuthally isotropic so that it can be treated as a circular aperture or antenna with radial symmetry. Under these assumptions, terms like Δx in the previous section can be replaced by Δr.

For convenience, we normalize the anchoring roughness parameters (ν, s, ξ) to the scale of the wavelength and define them to be the "wavelength-scaled" or "scaled" roughness parameter, e.g., scaled RMS slope, $s_\lambda = s(\lambda)$; scaled RMS height, $\xi_\lambda = \xi(\lambda)$; and scaled RMS deviation, $\nu_\lambda = \nu(\lambda)$. From Eq. (1c) we can also write the scaled-RMS slope as

$$s_\lambda = \frac{\nu(\lambda)}{\lambda} = \frac{\nu_\lambda}{\lambda}. \tag{4}$$

Normalizing in this fashion has no effect on our assumptions about the roughness of the surface; it is, however, a very convenient natural scale length for our derivation. The physical interpretation of the scaled RMS slope will also be very important later. In essence, it is the RMS slope that would be measured by a field worker using a ruler of length λ.

Throughout the following, we will often discuss the phenomenon of wave interference. To clarify our terminology, consider the interference of two fields of the same wavelength, λ, and amplitude, E_1 and E_2 (we retain separate subscripts only to distinguish between the two waves). If the two fields are exactly in phase (e.g., they originate from the same source and follow similar path lengths), they constructively interfere and their time-averaged combined field is

$$E_{\text{Total}} = E_1 + E_2 > 0; \tag{5a}$$

i.e., the sum of the fields is always greater than 0. The power from the combined fields is

$$P = (E_1 + E_2)^2 = E_1^2 + E_2^2 + 2E_1E_2 \tag{5b}$$

and the cross-term ($2E_1E_2$) represents the increase in field strength due to mutual constructive interference. If, however, the phases between the two fields are randomized (e.g., they originate from independent and uncorrelated sources), then the time averaged field is

$$E_{\text{Total}} = 0 \tag{5c}$$

because the randomized phases tend to cancel one another. However, the power from the combined fields is not zero but given by

$$P = (E_1 + E_2)^2 = E_1^2 + E_2^2. \tag{5d}$$

Only the cross-term ($2E_1E_2$) is zero. We will loosely use the term "coherent" to refer to echoes composed of constructively interfering fields (in any significant measure) and the term "incoherent" to refer to echoes composed of randomly interfering fields.

B. The Huygens Wavelet Methodology

The use of Huygens wavelets to solve problems in diffraction and antenna theory is well established and is the underlying basis of Fresnel–Kirchhoff integral solutions (cf. Ulaby *et al.* 1981, Goodman 1968, Gaskill 1978). Conceptually, we may view a propagating electromagnetic wave as a source which, at each point in space, generates a new spherical wave. The interference of these new wavelets gives rise to a new wave front, and this continues ad infinitum. In diffraction problems, an incident wave is blocked by an obstruction and only generates spherical wavelets within the confines of an aperture or opening within that obstruction. The associated diffraction pattern opposite the aperture is the result of the interference between the wavelets arising from the continuous, but finite, aperture area. Similarly, in antenna theory, each point on the antenna is viewed as an independent source of spherical wavelets, and their mutual interference gives rise to the antenna beam pattern.

Mathematically, the solution of diffraction or antenna problems of this type involves integrating the amplitude and phase of all wavelets to determine the angular amplitude function of the resultant electromagnetic field. Under the conditions assumed in this paper, most critically the far-field approximation, it can be shown that the resultant electromagnetic field is proportional to the Fourier transform (or, where circular symmetry is invoked as it is here, the equivalent Fourier–Bessel or Hankel transform) of the aperture or antenna shape (Goodman 1968). Specifically,

$$E = \frac{j}{\lambda Z}\exp[-jkZ]\left(\frac{1+\cos\theta}{2}\right)E_0\mathcal{H}_0(A), \tag{6}$$

where j is the root of -1, Z is the distance of the observation plane from the aperture or antenna, k is the wavenumber $(2\pi/\lambda)$, θ is the scattering angle, E_0 is the amplitude of the incident field, $\mathcal{H}_0$ is a Fourier–Bessel or zeroth-order Hankel transform, and A is a function describing the shape and transmission (or scattering) properties of the aperture (aperture function). The cosine term in parentheses is called the obliquity factor, and for near-nadir observations ($\theta < 20^\circ$), it can be ignored with insignificant error. In essence, Eq. (6) represents a complex Huygens wavelet (first two terms) modified by the Fourier–Bessel transform of the aperture or antenna shape. The quantity measured by a receiver is the radiated "power density" (W/m^2), given by

$$P = \frac{1}{2\eta}|EE^*|, \tag{7}$$

where η is the impedance of free space (Ulaby *et al.* 1981).

In the following sections, we develop the near-nadir coherent backscatter cross-section of a self-affine fractal surface in steps, beginning with a smooth conducting surface. We will hereafter refer to the process as one of scattering, i.e., absorption of a plane wave by individual points and reemission as a wavelet, and note modifications to the above mathematical treatment where required to maintain consistency with the scattering geometry.

C. Scattering from a Smooth, Conducting Surface

For a circular surface (or plate), Eq. (6) is written

$$E_{\text{circ}} = \frac{j}{\lambda Z}\exp[-jkZ]E_0\mathcal{H}_0(\text{circ}(r_0)), \tag{8a}$$

which is equivalent to

$$E_{\text{circ}} = \frac{j}{\lambda Z}\exp[-jkZ]E_0\pi r_0^2\frac{2J_1(kr_0\sin\theta_e)}{kr_0\sin\theta_e}, \tag{8b}$$

where circ is the "circular" function (circ = 1 for $r \le r_0$ and circ = 0 for $r > r_0$), θ_e is the emission or scattering angle (measured from nadir, always positive), and J_1 indicates a first-order J–Bessel function. The associated power density of Eq. (8b) is called the Airy pattern (Gaskill 1978, Ulaby *et al.* 1981).

Equations (8) are based on the assumption that a plane wave is normally incident upon the surface. For an obliquely incident wave, we must account for the phase change that occurs as it impinges upon the surface. It can be shown that the solution to a more general bistatic case (source and receiver in the principal plane) is

$$E_{\text{circ}} = \frac{j}{\lambda z}\exp[-jkz]E_0\pi r_0^2\frac{2J_1(kr_0(\sin\theta_e - \sin\theta_i))}{kr_0(\sin\theta_e - \sin\theta_i)}, \tag{9}$$

where θ_i is the incidence angle (from nadir, positive when opposite the scattering angle, i.e., forward scattering direction; negative when on the same side as the scattering angle, i.e., backscattering direction). Equation (9) reduces to Eq. (8b) for normal illumination ($\theta_i = 0$). The effect of the modification to Eq. (9) is to make a specular "lobe" in the forward scattering direction when illuminated off-nadir and to reduce the scattered

field (and power) more rapidly than Eqs. (8) in the backscattering direction. Note that the angular width of the scattered lobe is a function of the surface size, r_0: a small surface has a very wide, low amplitude lobe, while a large surface has a very narrow, high amplitude lobe. In the limit of an infinite half-plane, the lobe becomes a delta function with no angular width, i.e., purely specular. One may envision this latter case as an infinite number of spherical wavelets constructively interfering to produce a reflected plane wave.

D. Scattering from a Smooth, Circular Dielectric Surface

In the case of scattering from a smooth *dielectric* plate of radius r_0, the electric field in the principal plane far-zone is given by

$$E_{\text{diel,circ}} = \frac{j}{\lambda Z}\exp[-jkZ]RE_0\pi r_0^2\frac{2J_1(kr_0(\sin\theta_e-\sin\theta_i))}{kr_0(\sin\theta_e-\sin\theta_i)}, \tag{10}$$

where R, which we call the "effective reflectance amplitude," is a function giving the fraction of power reflected from the surface, $0 \le R \le 1$. For a perfectly smooth dielectric surface, the function R is given by the Fresnel reflection coefficient and is a function of the incident and emission angle as well as the dielectric constant. For the case of normal incidence,

$$R_{\text{Fresnel}} = \frac{\varepsilon^{1/2}-1}{\varepsilon^{1/2}+1}, \tag{11}$$

where ε is the dielectric constant, and we have assumed a magnetic permeability ~ 1 (Ulaby *et al.* 1981). We assume that R_{Fresnel} remains approximately constant and equal to Eq. (11) for near-nadir scattering.

E. Scattering from a Roughened (Stationary) Dielectric Surface

For the problem of near-nadir reflection from a stationary randomly rough surface (of any given shape), the aperture function is modified by a random phase retardation. The solution is essentially the same as those discussed above, except that the amplitude of the scattered electric field is modified by the Fourier transform of the phase density function (or characteristic function in statistics literature). For a *stationary* dielectric surface whose roughness (or phase retardation function) is given by a Gaussian distribution of heights with RMS height of ξ, the coherent scattered field is given by

$$E_{\text{rough,diel}} = \exp[-2k^2\xi^2\cos^2\theta]E_{\text{smooth,diel}}. \tag{12}$$

The characteristic function in Eq. (12) (exponential term) is closely related to the well-known Rayleigh roughness criterion and is discussed by Beckmann and Spizzichino (1963) and Barrick and Peake (1967). Note that the coherent scattered electric field will only be significant for values of ξ which are small relative to λ, and therefore Eq. (12) only represents the constructive interference cross-terms illustrated by Eqs. (5a) and (5b). For large ξ, there is no constructive interference (only randomized phase relations), and the scattered field and power are incoherent and analogous to that given by Eqs. (5c) and (5d).

Barrick and Peake (1967) restrict the use and application of Eq. (12) for surfaces that are "slightly rough," in the same sense that we discussed in the previous paragraph. However, what is lacking in their and subsequent analyses is the *horizontal scale* at which the surface roughness is measured or defined. We will argue that the relevant horizontal scale is the wavelength of the incident energy. As noted earlier, a fractal surface can be relatively smooth at the wavelength scale (e.g., 12 cm for S-band) and become incredibly rough at larger scales, or not, depending upon the Hurst exponent. This allows us to examine a continuum of surface roughness types, from very smooth to very rough, with the same model. We will also make an assumption, first invoked by Hagfors (1964) and later by Barrick and Peake (1967), that small-scale roughness (below the Rayleigh criterion) does not significantly affect the angular scattering function of the coherent echo. In his discussion of this assumption, Hagfors (1964) treated the incident wave as a type of smoothing filter. Although this assumption precludes rigorous treatment of the scattered field (i.e., it disregards the common physical optics assumption of a well-behaved or gently undulating surface), it is not without some empirical basis. Opticians frequently polish optical surfaces to a geometric figure, accurate to within a fraction of a wavelength of incident light. The exact nature of the deviations at this scale is unimportant to the final optical performance.

Barrick and Peake (1967) state that, for surfaces obeying Eq. (12), our model parameter (Eq. 10) $R = R_{\text{Fresnel}}$. For reasons to be discussed below, we believe that the Fresnel reflection coefficient is an upper bound for the effective reflectance amplitude, and that in general, R will differ from R_{Fresnel} by a depolarization factor that is a function of wavelength and dielectric constant. While this additional factor will modify the magnitude of our model solutions, it will not affect their shape or width.

F. Scattering from a Roughened Self-Affine Dielectric Surface

We now extend the problem to one of scattering from a surface which is roughened and self-affine, i.e., nonstationary, and account for the functional dependence of RMS height and deviation with scale in the following manner. For any and every point on the surface, we may define a series of concentric thin annuli of increasing radii, r_a. For convenience, we will discuss only one such arbitrary point and associated annuli. As we move outward from the center point, Eqs. (2) indicate that the RMS deviation, $\nu(r_a)$, relative to the center will increase. By definition, all of the points in any given annulus are Gaussian distributed with RMS height ξ proportional to ν at that radius,

$$\xi(r_a) = \frac{1}{\sqrt{2}}\nu_\lambda\left(\frac{r_a}{\lambda}\right)^H, \tag{13}$$

and we have chosen (for convenience) our reference length to be one wavelength. The factor of $\sqrt{2}$ is a required constant of

proportionality that can be theoretically derived (cf. Shepard *et al.* 1995 and references therein). Equation (13) allows us to think of a nonstationary surface in a new way—as an infinite number of points, each with an associated collection of concentric annuli which individually have a constant RMS height (i.e., are stationary), but collectively represent a surface with an RMS height that increases with distance from each point.

From Eqs. (6) and (12), the coherent scattered field from any roughened (stationary) annulus of radius $r_a(\delta(r - r_a))$ is

$$E_{\text{rough,annulus}} = \frac{j}{\lambda Z}\exp[-jkZ]\exp[-2k^2\xi^2\cos^2\theta] \times RE_0\mathcal{H}_0[\delta(r - r_a)], \quad (14a)$$

where ξ is the RMS height of the given annulus. For the general case of bistatic scattering in the principal plane, Eq. (14a) can be written

$$E_{\text{rough,annulus}} = \frac{j}{\lambda Z}\exp[-jkZ]\exp[-2k^2\xi^2\cos^2\theta_e] \times RE_0 kr_a J_0(kr_a(\sin\theta_e - \sin\theta_i))\,dr_a, \quad (14b)$$

or for the specific case of backscattering,

$$E_{\text{rough,annulus}} = \frac{j}{\lambda Z}\exp[-jkZ]\exp[-2k^2\xi^2\cos^2\theta_i] \times RE_0 kr_a J_0(2kr_a\sin\theta_i)\,dr_a, \quad (14c)$$

where J_0 is a zeroth-order J–Bessel function. From this point on, we shall only consider backscattering solutions since that is our principal interest and drop the subscript on θ for succinctness.

Babinet's Principle states that the diffracted E-field of an arbitrary aperture can be found by summing the diffracted E-fields of many smaller apertures that, all together, are equivalent in area and shape to the larger aperture (Klein 1970). Therefore, to find the coherent E-field scattered from the entire illuminated roughened area about any given point, we sum the E-fields from all the annuli around any single point on the surface:

$$E = \frac{j\lambda}{Z}\exp[-jkZ]2\pi RE_0 \times \int_{\hat{r}=0}^{\infty}\exp[-8\pi^2(\xi/\lambda)^2\cos^2\theta]\hat{r}\,J_0(4\pi\hat{r}\sin\theta)\,d\hat{r}. \quad (15)$$

Note in Eq. (15) that we have explicitly written out the wavenumber, k, inside the integral and introduced a new variable of integration given by

$$\hat{r} = \frac{r_a}{\lambda}, \quad (16)$$

which, again, normalizes all measurements to wavelength units. Further, we have assumed the illuminated area to be infinite in extent ($\hat{r} \to \infty$).

On a self-affine surface, the RMS height in Eq. (15) is also a function of scale, and we may calculate the coherent angular scattering function from any point on a surface given its Hurst exponent (or fractal dimension from Eq. 3), scaled RMS deviation and/or slope, and scattering angle by combining Eqs. (4), (13), and (15):

$$E = \frac{j\lambda}{Z}\exp[-jkZ]2\pi RE_0 \times \int_{\hat{r}=0}^{\infty}\exp\left[-4\pi^2 s_\lambda^2\hat{r}^{2H}\cos^2\theta\right]\hat{r}\,J_0(4\pi\hat{r}\sin\theta)\,d\hat{r}. \quad (17)$$

In the event that a surface is better represented by two or more Hurst exponents at different ranges in scale, the constant H in Eq. (17) should be replaced by $H(\hat{r})$.

Equation (17) represents the enhancement in scattering, relative to an isotropic Huygens wavelet, that takes place from every point on the surface due to constructive interference by its nearest neighbors. On a nonstationary surface, constructive interference (coherence) is only significant between wavelets that originate from points close together. Points separated by a great distance are statistically independent, because the RMS height is scale-dependent, and randomly interfere. This differs in a subtle but significant way from the more traditional view that points separated by a distance greater than the autocorrelation length will randomly interfere. Recall that models invoking this mechanism assume stationary surface behavior and thus every annulus on such surfaces will have the same RMS height. As we will elucidate in more detail below, the model proposed here leads to the concept of a coherent patch or "effective aperture" for each point on the surface. Because the region surrounding various points on the surface is statistically identical, the backscatter cross-section of the entire surface is enhanced, relative to an isotropically scattering surface, by the same factor as its individual scattering elements are to a Huygens wavelet.

Equation (17) can be evaluated in a closed form for three cases: $H = 0.0 (D = 3.0)$, i.e., a stationary surface; $H = 0.5 (D = 2.5)$, i.e., a Brownian surface; and H = 1.0 ($D = 2.0$), a self-similar surface. In the first case, the exponential function becomes independent of $\hat{r}$ and comes out of the integral. The remaining integral is easily evaluated and gives an Airy pattern solution identical to Eqs. (10) as modified for roughness by Eq. (12). As previously noted, integrating over a surface of infinite extent results in a delta function of infinite magnitude and zero width. If such a surface is uniformly illuminated over an infinite area, the constructively interfering component of the scattered field will equal zero for any nonzero backscattering angle (although the randomly interfering, or incoherent, component of the field will remain nonzero).

For the case of a Brownian surface, $H = 0.5$, Eq. (17) is evaluated to give

$$E = \frac{j\lambda}{Z}\exp[-jkZ]RE_0\frac{s_\lambda^2\cos^2\theta}{8\left(\pi^2 s_\lambda^4\cos^4\theta + \sin^2\theta\right)^{3/2}} \quad (18a)$$

and a power density of

$$P = \frac{\lambda^2}{2\eta Z^2}\rho E_0^2 \frac{s_\lambda^4 \cos^4\theta}{64\left(\pi^2 s_\lambda^4 \cos^4\theta + \sin^2\theta\right)^3}, \qquad (18b)$$

where $\rho = R^2$ and is equivalent to the Fresnel power reflection coefficient in the limit as the surface becomes perfectly smooth.

For the case of a self-similar surface, $H = 1.0$, Eq. (17) leads to

$$E = \frac{j\lambda}{Z}\exp[-jkZ]RE_0 \frac{1}{4\pi s_\lambda^2 \cos^2\theta}\exp\left[\frac{-\tan^2\theta}{s_\lambda^2}\right] \qquad (19a)$$

and

$$P = \frac{\lambda^2}{2\eta Z^2}\rho E_0^2 \frac{1}{16\pi^2 s_\lambda^4 \cos^4\theta}\exp\left[\frac{-2\tan^2\theta}{s_\lambda^2}\right]. \qquad (19b)$$

G. The Effective Aperture

For surfaces with Hurst exponents other than zero, i.e., nonstationary, the solution to Eq. (17) is finite in amplitude and width, even when integrating to infinite surface scales, because the surface roughness at some annular radius eventually increases to a value where there is no further significant constructive interference [see Eqs. (12) and (13)]. The area around each point on the surface covered by all the annuli up to and including this radius we call the effective aperture since it defines the approximate limits of the region contributing to the coherent near-nadir echo. We define this radius to be the distance at which the annular constructive interference becomes less than e^{-n}, where n is a constant. Combining and rewriting Eqs. (12) and (13) yields

$$\hat{r}_{\text{eff}} = \left[\frac{n}{4\pi^2 s_\lambda^2 \cos^2\theta}\right]^{\frac{1}{2H}}, \qquad (20)$$

where $\hat{r}_{\text{eff}}$ is in units of wavelength. We prefer to set $n = 5$, the point at which the constructive addition has dropped to ~1%. This corresponds to the annular radius at which the RMS height becomes approximately one-quarter wavelength—about the Rayleigh criterion.

To illustrate Eq. (20), consider a surface with scaled RMS slope, $s_\lambda = 0.2$ (~11°) (Fig. 3). This value is typical of smooth pahoehoe lava flows measured at S-band (12 cm) scales (cf., Campbell and Shepard 1996). For this surface with Hurst exponents of 0.2, 0.5, and 0.8, the effective apertures are ~18 λ (2.1 m), ~3 λ (0.36 m), and ~2 λ (0.24 m), respectively (note that only the $H = 0.2$ surface resembles a pahoehoe). It is apparent that the Hurst exponent plays a major role in determining the size of the effective aperture, which in turn affects the magnitude and width of the resulting scattered field.

It should also be noted that the effective aperture is wavelength-dependent because the surface roughness parameter, s_λ, is measured at the wavelength scale. If we consider the above surface illuminated by an L-band (24 cm) wave, the scaled RMS slope differs significantly from that at S-band scales. For the same surfaces as above ($H = 0.2$, 0.5, and 0.8), the values for s_λ are 0.11 (6°), 0.14 (8°), and 0.17 (10°), respectively (see Eq. 2c). Note in each case that the scaled RMS slope is less at L-band than at S-band. The effective apertures at L-band for these three cases are ~296 λ (71 m), 6.5 λ (1.6 m), and 2.5 λ (0.6 m), respectively.

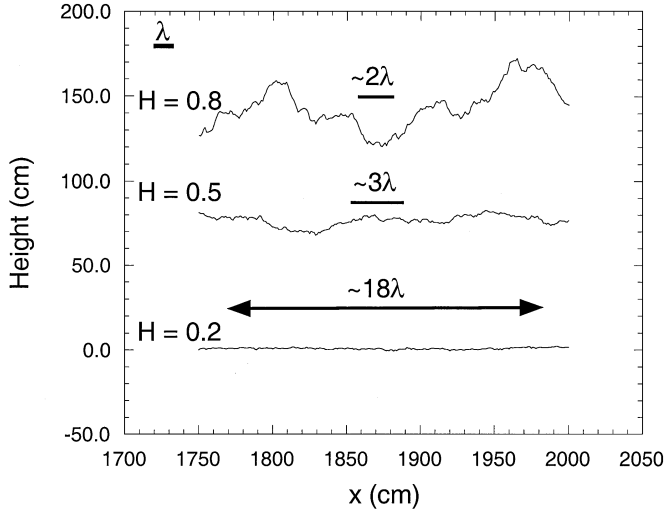

FIG. 3. Three profiles of surfaces with $H = 0.8$ (top), 0.5 (middle), and 0.2 (bottom). The scaled RMS slopes of each profile are identical and equal to 0.2 (11°) at the 12-cm scale (S-band). The wavelength is shown for scale in the upper left corner. The lines above each profile represent the size of the effective aperture of those particular profiles. The roughest surface at meter scales ($H = 0.8$) has the smallest effective aperture (~24 cm or two wavelengths) and would display only a weak coherent near-nadir echo. The smoothest of the three at meter scales ($H = 0.2$) has a large effective aperture (~18 wavelengths) and would display a significant near-nadir coherent echo.

H. Backscatter Cross-Section of a Self-Affine Dielectric Surface

The backscatter cross-section of a surface is defined as the ratio of power density scattered from that surface to the power density scattered from a perfect isotropic scatterer of the same area, at the same distance, and under the same illumination and viewing conditions (Elachi 1987, Ulaby *et al.* 1981). The power density of such a scatterer is

$$P_{\text{iso}} = \frac{\lambda^2 E_0^2}{(2\eta)4\pi Z^2}. \qquad (21)$$

For the closed forms above [Eqs. (18) and (19)], we can therefore write the backscatter cross-section, σ_0, as

$$\sigma_0(H = 0.5) = \frac{\rho\pi s_\lambda^4 \cos^4\theta}{16\left(\pi^2 s_\lambda^4 \cos^4\theta + \sin^2\theta\right)^3} \qquad (22)$$

and

$$\sigma_0(H = 1.0) = \frac{\rho}{4\pi s_\lambda^4 \cos^4\theta}\exp\left[-\frac{2\tan^2\theta}{s_\lambda^2}\right]. \qquad (23)$$

For the general case, we can write the backscatter cross-section as

$$\sigma_0(H) = 16\pi^3\rho \times \left[\int_{\hat{r}=0}^{\infty} \exp\left[-4\pi^2 s_\lambda^2 \hat{r}^{2H}\cos^2\theta\right]\hat{r}\,J_0(4\pi\hat{r}\sin\theta)\,d\hat{r}\right]^2. \quad (24)$$

I. Similarities to Current/Previous Models

Both Eqs. (22) and (23) exhibit interesting similarities to previous work. Equation (23) is a Gaussian function, similar to the one derived by Hagfors (1964) (see also Hagfors and Evans 1968) for a surface with Gaussian height distribution and Gaussian autocorrelation function, and to the Gaussian distributed facet model utilized by Simpson and Tyler (1982). Equation (22) displays interesting similarities to the commonly used Hagfors (1964) solution for a surface with Gaussian height distribution and exponential autocorrelation function, approximated as a linear function near the origin

$$\sigma_0(\theta) = \frac{\rho C}{2}(\cos^4\theta + C\sin^2\theta)^{-3/2}, \quad (25)$$

where the roughness parameter, $C^{-1/2}$, is defined as

$$C^{-1/2} = 4\pi\frac{\xi^2}{l\lambda} \quad (26)$$

and l is the autocorrelation length of the surface. In our solution, πs_λ^2 appears to be analogous to $C^{-1/2}$ (although we do not care to attach a physical interpretation to this grouping of parameters) and our denominator is cubed where Hagfors' is raised to $3/2$ power. Equation (22) also displays interesting similarities to the Muhleman (1964) geometric optics model, specifically the cubic denominator of sine and cosine terms. And, as we will see below, numerical solutions to Eq. (24) using intermediate forms of H (especially $H < 0.5$) are very close in shape to the commonly used exponentially distributed facet model (Simpson and Tyler 1982). The similarity of our model solutions to these equations is not singular. In the next section, we demonstrate that our model comprises a *family* of functions that smoothly transition between Gaussian, Hagfors-like, and exponential-like scattering behaviors.

With these similarities noted, however, we do not wish to leave the reader with the impression that the above models are endmembers, in any sense, to the model derived here. While specific examples of similar form can be found, there are no simple relationships between the roughness parameters used in our model and those above. The basic physics of scattering is the same; however, the fractal surface model utilized here is based on observed surface behavior and is fundamentally different than any previously used. One possible explanation for the observed similarities is that the models discussed above have all survived a type of selection process; those models that successfully fit observed data were retained; those that did not were discarded. Therefore, similarities between this and previous models are probably coincidences of functional form that have been selectively winnowed by comparisons with observed data.

V. DISCUSSION

Having derived the near-nadir scattering behavior of a self-affine surface in the previous section, we now wish to briefly discuss the model and its properties in a larger context and address the questions posed in the Introduction.

A. Interpretation of RMS Slope Inferred from Radar Backscatter

The model derived above and given by Eqs. (22)–(24) indicates that the near-nadir angular scattering function is strongly controlled by constructively interfering wavelets from an area of the surface approximated by the effective aperture. Typical radii for this area range from a few to hundreds of wavelengths. Interestingly, one of the two major surface roughness parameters that determines the effective aperture is the wavelength-scaled surface RMS slope, s_λ (or other appropriately scaled roughness parameter). In previous work, we demonstrated that the off-nadir diffuse return could also be directly correlated with the wavelength-scaled surface roughness (Campbell and Shepard 1996). Taken together, these works suggest that the surface scattering process is completely controlled by the wavelength-scaled surface roughness and its scaling behavior.

One intriguing result of this model is that it predicts a significant quasi-specular echo *only* for surfaces that are relatively smooth at the wavelength scale and does so without assuming a well-behaved or gently undulating surface. A surface with a scaled RMS slope of 20° will have a scaled RMS height of about one-quarter wavelength and an effective aperture on the order of one wavelength. At this roughness and higher, the model predicts essentially no coherent echo. Therefore, surfaces which exhibit significant near-nadir echoes are predicted either to be relatively smooth at the wavelength scale or to contain areas that are relatively smooth.

Another intriguing component of this model is the physical link between the radar-derived wavelength-scaled roughness and the surface topography. In essence, the radar wave appears to be acting as a "ruler" with which we measure surface roughness—the same roughness one measures in a topographic survey. Observations at a single wavelength give us a snapshot of the surface statistical properties at scales from below the wavelength up to (approximately) the effective aperture. Using observations made of the same area at different wavelengths, it may be possible to construct a statistical picture of the surface morphology which can be directly compared with the same scale-dependent statistics measured on terrestrial analogs.

Based on this and previous work, we suggest that the scattering process may be visualized in the following way. The near-nadir echo is dominated by constructive interference

(coherent or quasi-specular echoes) because the paths traveled by waves on any given wavefront (or equivalently the phase changes in those waves) are modified primarily by variations in surface height. In the event that the surface is rough at the wavelength scale ($\xi_\lambda > \lambda/4$), no significant coherent echo will occur. As the incidence angle increases, the paths traveled by waves on any given wavefront vary systematically with their lateral location *in addition to* the random variations in surface height. The returned echoes will be increasingly dominated by random interference between wavelets separated in phase (incoherent or "diffuse" echoes) as the incidence angle is increased. Although many aspects of the scattering process, including polarization states, must be worked out to quantify this kind of model, we believe it is a simpler and more satisfying view than the more traditional one of two separate scattering regimes.

B. Interpreting the Shape and Width of the Near-Nadir Echo

The analytical solutions given by Eqs. (22) and (23) and numerical solutions to Eq. (24) suggest that the shape of the angular backscattering function is controlled primarily by the Hurst exponent or fractal dimension and secondarily by the wavelength-scaled roughness. Figure 4A shows the range in angular scattering behaviors observed for surfaces with the same value of s_λ but varying H. Note the change in shape from Gaussian-like (concave down) for surfaces with large values of H to forms similar in shape to the Hagfors (concave up) and exponential (linear) functions at lower values of H. Figure 4B shows the ability of our model to mimic the Hagfors (1964) angular scattering function. Our model never looks exactly like an exponential function at the origin, i.e., a sharp, discontinuous derivative, but instead always rolls over near the origin like the Hagfors and Gaussian functions. The tail, however, can take shapes similar to the Gaussian, exponential, and Hagfors functions.

The magnitude of the angular scattering behavior is a function of the wavelength-scaled RMS slope and effective aperture, the latter of which is controlled by the combination of Hurst exponent and scaled RMS roughness parameters through Eq. (20). This can be easily understood if one views the area defined by the effective aperture as analogous to a hole through which a virtual source is being diffracted or as the diameter of a transmitting antenna. The larger the aperture and the smaller the wavelength-scaled roughness, the narrower the scattered lobe and the greater its magnitude (the magnitude will increase approximately as r_{eff}^2.) The largest effective apertures occur with surfaces that have low values of H (high fractal dimensions) and low scaled RMS slopes (see Fig. 3). The smallest effective apertures occur with surfaces that have high values of H (Fig. 3). This can be understood by recalling that fractal surfaces with low values of H will roughen at a slower rate than those with high H. Therefore, for a given value of s_λ (or ν_λ), a greater distance to the outer annulus is required of a low H surface before the constructive interference decreases below 1%.

It is interesting to compare the above shape and roughness interpretations with historical accounts of the best-fit scattering functions to various planetary surfaces. Tyler *et al.* (1992) note that, on Venus, the best-fit angular scattering function for the majority of the planetary surface is exponential in form. They further note that near-nadir echoes best fit by a Hagfors model tend to correlate with the smoothest areas, while echoes best fit by a Gaussian model tend to correlate with the roughest areas. Similar trends and correlations were observed for the Moon by Simpson and Tyler (1982) with the exception that the most common best-fit angular scattering function was the Hagfors model. Based on the previous discussion, we expect the roughest surfaces at wavelength and higher scales to have the highest Hurst exponents (see Fig. 2) and Gaussian-like angular scattering functions. The smoothest surfaces at wavelength and higher scales will have the lowest Hurst exponents and have Hagfors

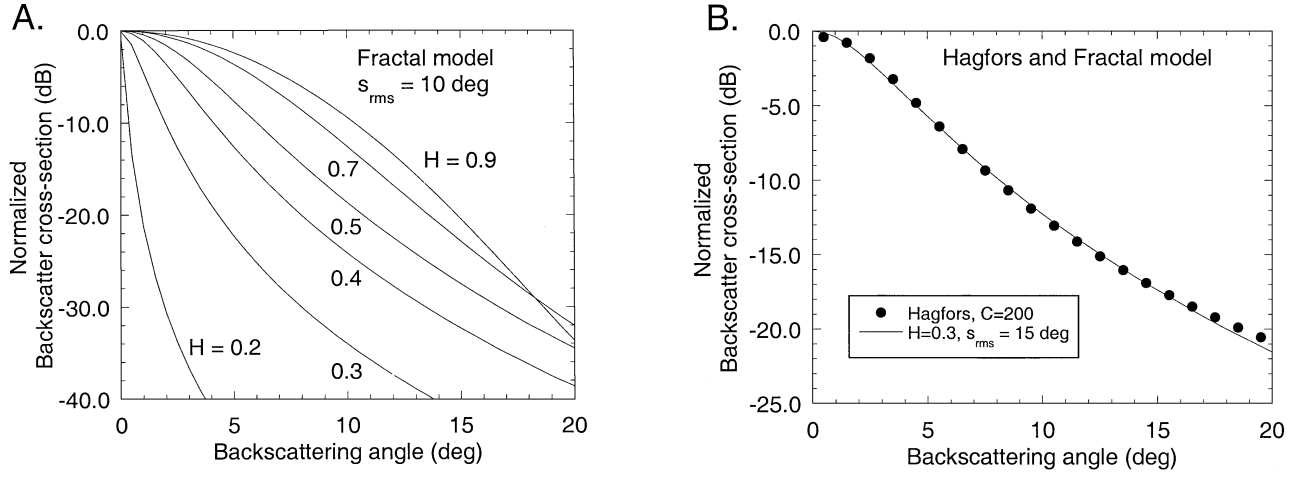

FIG. 4. (A) Normalized near-nadir angular scattering behavior for self-affine surfaces. Each surface has the same RMS slope measured at the scale of the wavelength (10°), but different Hurst exponents. Note the transition from convex down, Gaussian-like behavior to behaviors reminiscent of exponential and Hagfors behavior. (B) Illustration of our model's ability to mimic a typical Hagfors model ($C = 200$).

to exponential-like angular scattering functions. It is also reasonable to expect the most common angular scattering shape to be Hagfors or exponential because very rough surfaces will not have coherent near-nadir echoes.

C. The Wavelength Dependence of Radar Backscatter

The final problem we address is the question of how the inferred RMS slope varies with the wavelength of the incident radar. Figure 5 shows several views of two synthetic profiles which have the same Hurst exponent ($H = 0.5$) but which differ in roughness by a factor of 2. Both profiles are sampled at the 1-cm scale. The raw data in Fig. 5A illustrate a common method of display for this type of data in which the vertical (or y) axis is exaggerated. We have added horizontal lines at the maximum and minimum for each profile to emphasize the roughness differences between them. The profile on the top is obviously smoother than the profile on the bottom.

The second and third profiles down (Figs. 5B and 5C, respectively) are portions of the same profiles, plotted with no vertical exaggeration; the second shows a 50-cm portion of the smoother profile, and the third shows a 200-cm portion of the rougher profile. If we use their aspect ratios (max − min/profile length) as a measure of roughness, the two profiles (Figs. B & C) look remarkably similar and, in fact, are statistically the same. If we now take the position that the incident wave is acting as a kind of ruler and is sensitive to roughness as characterized by the RMS height/wavelength ratio, it becomes apparent that an incident 50-cm wave would view the smoother site (Fig. 5B) in the same way that an incident 200-cm wave would view the rougher site (Fig. 5C), and their respective near-nadir echoes would be the same. Note, however, that while the rougher site is only twice as rough as the smoother site, the wavelengths involved in this example differ by a factor of 4.

To state this relationship in a different way, when both a 50- and a 200-cm wave are scattered from the *same* surface, the 50-cm wave perceives the surface to be

$$\left(\frac{200}{50}\right)^{1-H} = 4^{1-H}$$

times *rougher* than the 200-cm wave. For a Brownian surface ($H = 0.5$), it looks twice as rough; for a stationary surface ($H = 0$), it appears four times as rough; and for a self-similar surface ($H = 1$), it looks identical to both waves.

The scale-dependent scattering behavior described above is a consequence of the self-affine nature of each profile. Because the near-nadir echo is a function of the roughness at the wavelength scale, i.e., by the roughness as perceived by the incident wave, we expect the RMS roughness inferred from backscatter observations to scale as the surface roughness, i.e., in a self-affine manner. This prediction is consistent with observations of the wavelength-dependence of scattering from the lunar surface (Simpson and Tyler 1982).

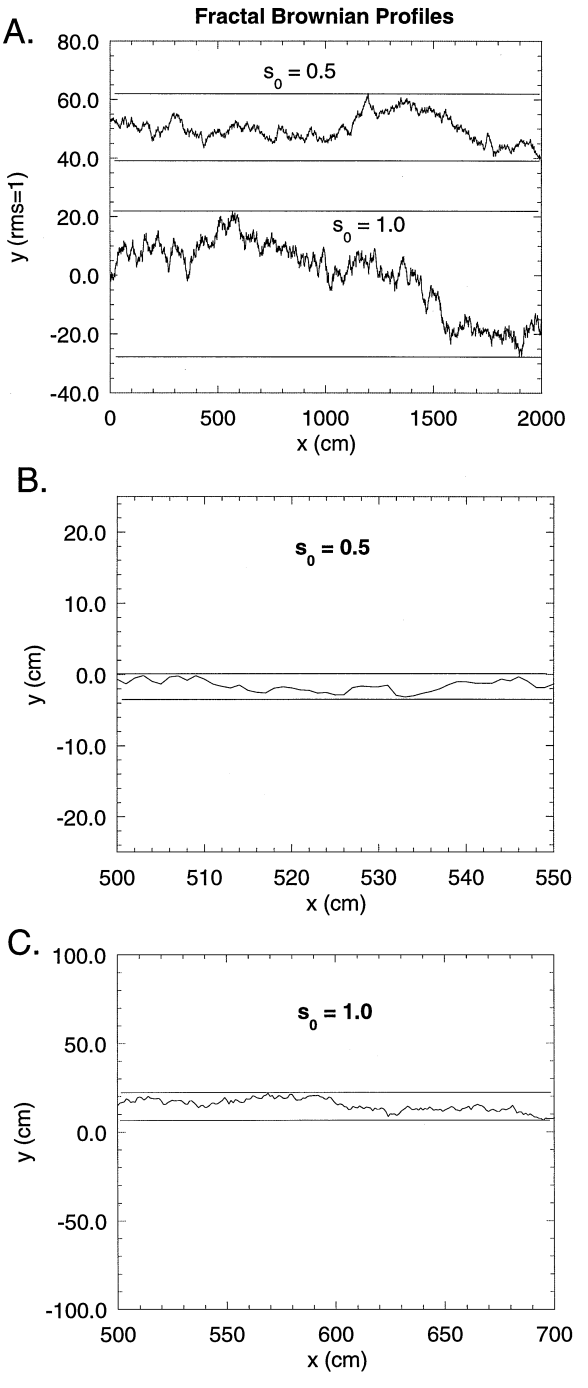

FIG. 5. (A) Brownian profiles ($H = 0.5$) with a factor of 2 difference in RMS slope at smallest scale (1 unit on x axis). The horizontal lines demarcate the range of extreme values and illustrate that the lower profile is twice as rough as the upper profile. Vertical exaggeration is the same for both profiles. (B) 50-cm subsection of the smoother profile, rescaled with no vertical exaggeration. Horizontal bars again demarcate the range of extreme values. (C) 200-cm subsection of the rougher profile, rescaled with no vertical exaggeration. Note that the profiles in (B) and (C) are statistically similar and have similar aspect ratios (or roughness) in their respective scales. This is a consequence of self-affinity and illustrates that a 200-cm wave would view the rough surface in the same way that a 50-cm wave would view the smoother surface, i.e., they would have identical angular scattering functions.

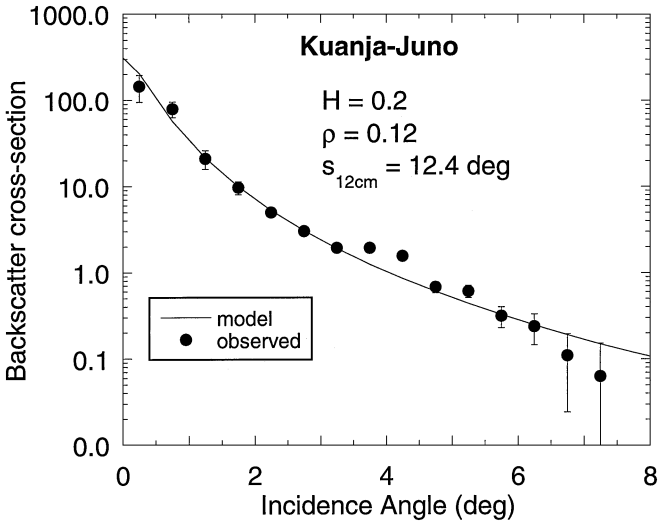

FIG. 6. Best-fit model curve to Magellan SCVDR data (20.0°S Lat., 107.0° Long.). The area was identified by Tyler *et al.* (1992) as extremely smooth based on a Hagfors model fit to the data. The Hurst exponent is very similar to those measured from extremely smooth pahoehoe flows and playas on Earth.

VI. ILLUSTRATION/APPLICATION

We now illustrate the model using scattering data derived by Tyler *et al.* (1992) from the Magellan altimeter experiment and published on the Magellan Surface Characteristics Vector Data Record (SCVDR) (Tyler *et al.* 1994). This data set represents the best estimate of the raw angular scattering behavior of the venusian surface. The data have a 0.5° angular resolution with the first data point at 0.25° incidence angle. The maximum incidence angle available is latitude-dependent and ranges from 4.5° at the poles to 10° for equatorial sites. Each "pixel" is approximately 16 km in diameter. Error bars are one standard deviation and we note that, by far, the largest uncertainties are associated with the first two points (0.25 and 0.75°), a result of fewer average "looks," off-nadir antenna pointing, and ranging uncertainties. Further information on the development of this data set can be found in Tyler *et al.* (1992).

Two areas were chosen to illustrate observed scattering behavior on Venus. One of the most interesting sites observed on the planet falls in an area between Kuanja and Juno Chasmata (20°S, 107°E). Tyler *et al.* (1992) noted this area to be the smoothest they observed with implied Hagfors RMS slopes of 0.5–0.7°. Our best-fit model to the data indicates a surface of very low H (0.20), with wavelength-scaled slopes of ~12° and effective reflectance of ~0.12 (Fig. 6). Although the wavelength-scaled RMS slope appears high, it must be remembered that this is the slope of the surface measured at 12 cm, and it is ultimately the value of H that controls the meter scale rough or smooth appearance of a surface. For comparison, these parameters are very similar to those measured from some areas of the Lunar Lake Playa, Nevada (discussed earlier), and extremely smooth Hawaiian pahoehoe flows (Fig. 7) (Arvidson *et al.* 1991, Campbell and Shepard 1996). In our preliminary search of the data, we find low H values (<0.5) to be very common in the plains, consistent with surfaces smooth at meter and higher scales.

Our second example is from an area in Vellamo Planitia (36.5°N, 170°E) and is typical of the average behavior observed throughout the venusian plains (Fig. 8). Although this surface is slightly smoother at the wavelength scale (11°), the higher value

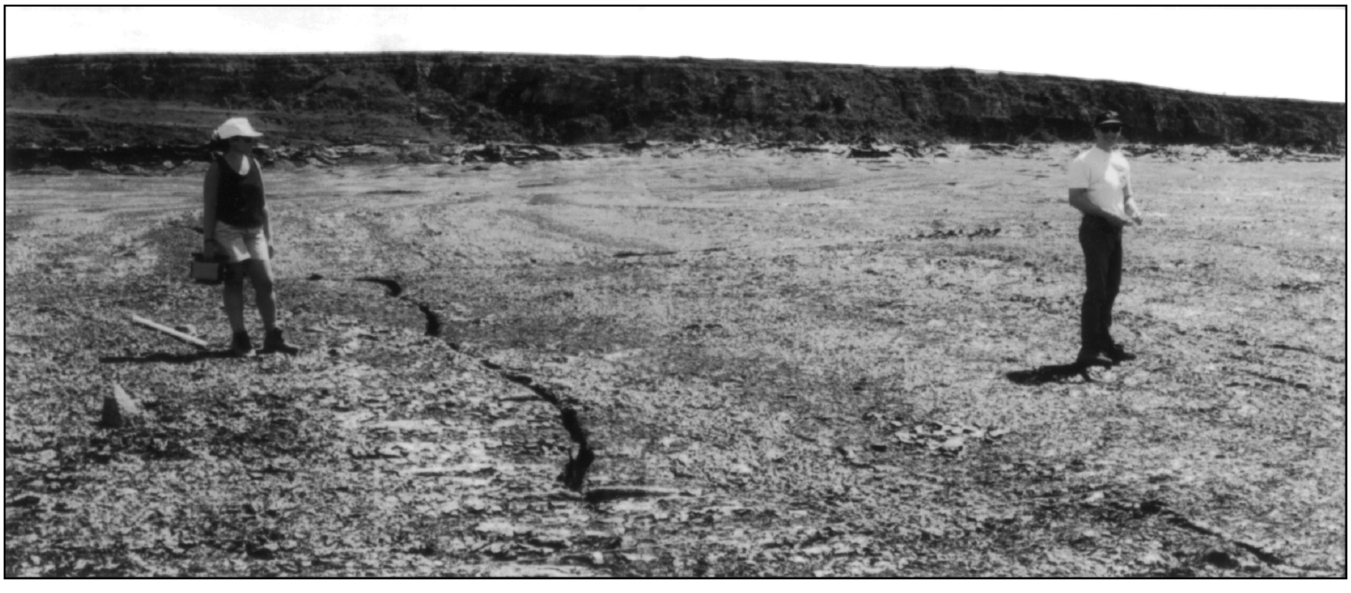

FIG. 7. Very smooth pahoehoe site with surface parameters, $H \sim 0.2$, $s_{12\ \mathrm{cm}} = 0.12$ (7°). Although this site is smoother at the wavelength scale than that inferred from the data fit in Fig. 5, the Hurst exponent is the same and ultimately controls the large scale topographic roughness.

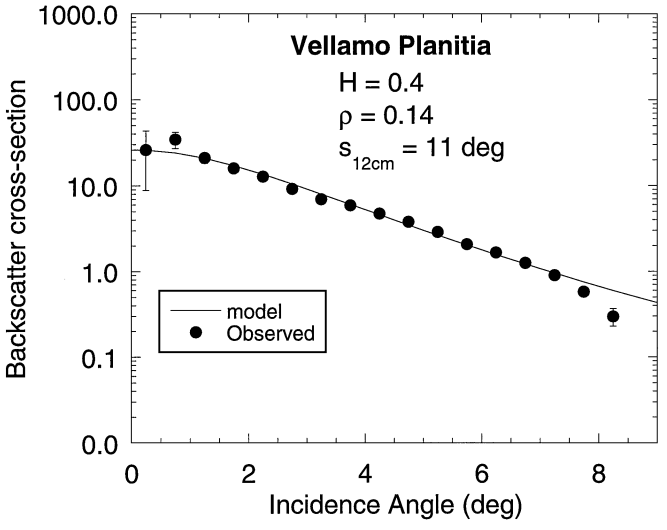

FIG. 8. Best-fit model curve to a typical Venus plains region (36.5N Lat., 170.0 Long.). This Hurst exponent and roughness are more typical of moderately smooth (terrestrial) pahoehoe flows (cf. Campbell and Shepard 1996).

of H (0.4) implies that it roughens more quickly with increasing scale than the previous example; at scales of 1 m and higher, this surface will be significantly rougher than the Kuanja–Juno site.

We have found that the backscattering behavior from some areas on Venus appears to be composite in form, i.e., an assortment of different surfaces combining to give a mixture of scattering behaviors. These observations often correlate with more Gaussian-like angular scattering shapes. Several workers (e.g., Simpson *et al.* 1977, McCollom and Jakosky 1993) have noted that inhomogeneities in surface statistics could lead to nonlinear mixtures of near-nadir scattering behavior. In the near-nadir regime ($\theta < 20^\circ$), the echo from a mixture of smooth and rough surfaces will give a disproportionate weighting to the smooth surface. Given the area covered by each SCVDR pixel ($\sim$250 km^2), this is not an unexpected observation and will be explored further in the future.

Our future work will also include a more comprehensive examination of the Magellan SCVDR data using this model, specifically in the extensive venusian plains where large regions of homogeneous terrain are more likely to occur. It will be of some interest to determine if systematic scaling differences exist in different plains regions and to compare those characteristics to measured terrestrial analogs. Additionally, we plan to perform first-order tests of the model using new multiwavelength data from the Moon and, where available, other targets of opportunity.

ACKNOWLEDGMENTS

This work was supported by NASA PG&G grants to both authors. The authors are grateful to R. Simpson for insightful discussions and thorough reviews of early versions of this work. We also thank Tor Hagfors and an anonymous reviewer for their constructive comments.

REFERENCES

Arvidson, R. E., M. A. Dale-Bannister, E. A. Guinness, S. H. Slavney, and T. C. Stein 1991. Archive of geologic remote sensing field experiment data, Release 1.0, NASA Planet. Data Syst. Jet Propulsion Laboratory, Pasadena, CA.

Barrick, D. E. 1970. Unacceptable height correlation coefficients and the quasi-specular component in rough surface scattering. *Radio Sci.* **5**, 647–654.

Barrick, D. E., and W. H. Peake 1967. Scattering from surfaces with different roughness scales: Analysis and interpretation. Rep. 1388-26, Ohio State Univ. Electrosci. Lab., Columbus, OH.

Beckmann, P., and A. Spizzichino 1963. *The Scattering of Electromagnetic Waves from Rough Surfaces.* Pergamon Press, New York.

Brown, S. R., and C. H. Scholz 1985. Broad bandwidth study of the topography of natural rock surfaces. *J. Geophys. Res.* **90**(12), 575–582.

Campbell, B. A., and M. K. Shepard 1996. Lava flow surface roughness and depolarized radar scattering. *J. Geophys. Res.* **101**, 18,941–18,951.

Campbell, B. A., R. E. Arvidson, and M. K. Shepard 1993. Radar polarization properties of volcanic and playa surfaces: Applications to terrestrial remote sensing and Venus data interpretation. *J. Geophys. Res.* **98**, 17,099–17,113.

Elachi, C. 1987. *Spaceborne Radar Remote Sensing: Applications and Techniques*. IEEE Press, New York.

Falconer, K. 1990. *Fractal Geometry: Mathematical Foundations and Applications.* Wiley, New York.

Farr, T. 1992. Microtopographic evolution of lava flows at Cima Volcanic Field, Mojave Desert, California. *J. Geophys. Res.* **97**, 15,171–15,179.

Gaskill, J. D. 1978. *Linear Systems, Fourier Transforms, and Optics*. Wiley, New York.

Goodman, J. W. 1968. *Introduction to Fourier Optics*. McGraw–Hill, San Francisco.

Hagfors, T. 1964. Backscattering from an undulating surface with applications to radar returns from the Moon. *J. Geophys. Res.* **69**, 3779–3784.

Hagfors, T. 1966. Relationship of geometric optics and autocorrelation approaches to the analysis of lunar and planetary radar. *J. Geophys. Res.* **71**, 379–383.

Hagfors, T., and J. V. Evans 1968. Radar studies of the Moon. In *Radar Astronomy* (J. V. Evans and T. Hagfors, Eds.), pp. 219–273. McGraw–Hill, New York.

Hastings, H. M., and G. Sugihara 1993. *Fractals: A User's Guide for the Natural Sciences*. Oxford Univ. Press, Oxford.

Helfenstein, P., and M. K. Shepard 1999. Submillimeter-scale topography of the lunar regolith. *Icarus* **141**, 107–131.

Klein, M. V. 1970. *Optics*. Wiley, New York.

Malamud, B., and D. L. Turcotte 1998. Self-affine time series. I. Generation and analysis. *Adv. Geophys.*, submitted.

Mandelbrot, B. B. 1967. How long is the coast of Britain? Statistical self-similarity and fractional dimension. *Science* **156**, 636–638.

Mandelbrot, B. B. 1982. *The Fractal Geometry of Nature*. Freeman, New York.

Mandelbrot, B. B., and J. R. Wallis 1995. Some long-run properties of geophysical records. In *Fractals in the Earth Sciences* (C. C. Barton and P. R. La Pointe, Eds.). Plenum Press, New York.

Mark, D. M., and P. B. Aronson 1984. Scale-dependent fractal dimensions of topographic surfaces: An empirical investigation, with applications in geomorphology and computer mapping. *Math. Geol.* **16**, 671–683.

McCollom, T. M., and B. M. Jakosky 1993. Interpretation of planetary radar observations: The relationship between actual and inferred slope distributions, *J. Geophys. Res.* **98**, 1173–1184.

Muhleman, D. O. 1964. Radar scattering from Venus and the Moon. *Astron. J.* **69**, 34–41.

Sayles, R. S., and T. R. Thomas 1978. Surface topography as a non-stationary random process. *Nature* **271**, 431–434.

Schroeder, M. 1991. *Fractals, Chaos, Power Laws: Minutes from an Infinite Paradise*. Freeman, New York.

Shepard, M. K., R. E. Arvidson, and E. A. Guinness 1993. Specular scattering from a terrestrial playa and implications for planetary surface studies. *J. Geophys. Res.* **98**, 18,707–18,718.

Shepard, M. K., R. A. Brackett, and R. E. Arvidson 1995. Self-affine (fractal) topography: Surface parameterization and radar scattering. *J. Geophys. Res.* **100**, 11,709–11,718.

Simpson, R. A., and G. L. Tyler 1982. Radar scattering laws for the lunar surface. *IEEE Trans. Antennas. Propag.* **AP-30**, 438–449.

Simpson, R. A., G. L. Tyler, and B. J. Lipa 1977. Mars surface properties observed by Earth-based radar at 70, 12.5, and 3.8 cm wavelengths. *Icarus* **32**, 147–167.

Turcotte, D. L. 1997. *Fractals and Chaos in Geology and Geophysics*, 2nd ed. Cambridge Univ. Press, New York.

Tyler, G. L., R. A. Simpson, and M. J. Maurer 1994. Magellan Project Global Vector Data Record, Release 1.0, NASA Planet. Data Syst. Jet Propulsion Laboratory, Pasadena, CA.

Tyler, G. L., R. A. Simpson, M. J. Maurer, and E. Holmann 1992. Scattering properties of the venusian surface: Preliminary results from Magellan. *J. Geophys. Res.* **97**, 13,115–13,139.

Ulaby, F. T., R. K. Moor, and A. K. Fung 1981. *Microwave Remote Sensing*, Vol. 1. Artech House, Norwood, MA.